

# Climate Diversity in the Habitable Zone due to Varying $pN_2$ Levels

Adiv Paradise<sup>a,b,\*</sup>, Bo Lin Fan<sup>d,e</sup>, Kristen Menou<sup>a,c</sup>, Christopher Lee<sup>d</sup>

<sup>a</sup>Department of Astronomy & Astrophysics, University of Toronto, St. George, Toronto, ON M5S 3H4, Canada

<sup>b</sup>Centre for Planetary Sciences, Department of Physical and Environmental Sciences, University of Toronto, Scarborough, ON M1C 1A4, Canada

<sup>c</sup>Physics & Astrophysics Group, Department of Physical and Environmental Sciences, University of Toronto, Scarborough, ON M1C 1A4, Canada

<sup>d</sup>Department of Physics, University of Toronto, St. George, Toronto, Ontario, M5S 1A7, Canada

<sup>e</sup>Department of Ecology & Evolutionary Biology, University of Toronto, St. George, Toronto, Ontario, M5S 3B2

---

## Abstract

A large number of studies have responded to the growing body of confirmed terrestrial habitable zone exoplanets by presenting models of various possible climates. However, the impact of the partial pressure of background gases such as  $N_2$  has been poorly-explored, despite the abundance of  $N_2$  in Earth's atmosphere and the lack of constraints on its typical abundance in terrestrial planet atmospheres. We use PlaSim, a fast 3D climate model, to simulate many hundreds of climates with varying  $N_2$  partial pressures, insolarations, and surface characteristics to identify the impact of the background gas partial pressure on the climate. We find that the climate's response is nonlinear and highly sensitive to the background gas partial pressure. We identify pressure broadening of  $CO_2$  and  $H_2O$  absorption lines, amplification of warming or cooling by the water vapor greenhouse positive feedback, heat transport efficiency, and cooling through Rayleigh scattering as the dominant competing mechanisms that determine the equilibrium climate for a given  $N_2$  partial pressure. Finally, we show that different amounts of  $N_2$  should have a significant effect on broadband reflected light observations of terrestrial exoplanets.

*Keywords:* terrestrial planets, atmospheres, habitability, climate

---

## 1. Introduction

The typical starting assumption for climate models of Earth-like planets is either a  $CO_2$ -dominated atmosphere like that on Mars and Venus, or an Earth-like atmosphere, with approximately 1 bar of  $N_2$ , trace  $CO_2$ , and a small amount of water vapor determined by evaporation and precipitation (e.g. Shields et al., 2016; Turbet et al., 2016; Boutle et al., 2017; Wolf, 2017). These are not unreasonable assumptions; our Solar System presents limited opportunities for in-depth studies of habitable zone terrestrial planets with atmospheres. Greenhouse gases like  $CO_2$ , rotation rate, eccentricity, and obliquity all have obviously strong effects on the climate (e.g. Manabe and Wetherald, 1975; Williams and Kasting, 1997; Shields et al., 2016; Haqq-Misra et al., 2018), and sophisticated climate models are computationally resource-intensive, limiting the number of models that can be included in sensitivity studies (e.g. Way et al., 2017).  $CO_2$  in particular has known geochemical processes which alter and constrain its atmospheric abundance in relation to other geophysical processes (Walker et al., 1981; Berner, 2004; Pierrehumbert, 2010; Valencia et al., 2018; Nakayama et al., 2019), which makes it an appealing parameter to vary for studies of both habitability and climate evolution (e.g. Koppurapu et al., 2013; Turbet et al., 2016; Paradise and Menou, 2017). While there has been considerable recent progress in understanding  $N_2$  geochemistry (Wordsworth, 2016),  $N_2$  is nonetheless less well-understood, and in addition is very difficult to observe with transit spectroscopy due to a lack of absorption lines at visible or infrared wavelengths (Benneke and Seager, 2012). We focus on  $N_2$  in this study, but this observational problem extends to all spectrally-inactive background gases. Because  $N_2$  is chemically mostly-inert and lacks absorption lines and therefore cannot directly act as a greenhouse gas, its dominant role in the climate is assumed to be as a

---

\*Corresponding author

Email address: paradise@astro.utoronto.ca (Adiv Paradise)

simple background gas pressure that keeps water liquid at Earth-like temperatures, enables heat transport, and causes pressure broadening of the CO<sub>2</sub> and H<sub>2</sub>O absorption lines (Kopparapu et al., 2014; Wordsworth, 2016; Olson et al., 2018; Ramirez, 2018).

However, there has been relatively little work exploring how different N<sub>2</sub> partial pressures (pN<sub>2</sub>) affect the climate, and existing work has not reached a consensus on the overall effect of N<sub>2</sub> on the climate. Nakajima et al. (1992) argued that increasing pN<sub>2</sub> (or the mass of any spectrally inactive and inert background gas) would likely lead to cooler climates, as the atmospheric lapse rate would trend towards the dry adiabat, resulting in more efficient cooling. Several studies (e.g. Goldblatt et al., 2009; Li et al., 2009; Charnay et al., 2013; Kopparapu et al., 2014; Wolf and Toon, 2014; Chemke et al., 2016) have shown that pressure-broadening of CO<sub>2</sub> by N<sub>2</sub> should lead to a stronger greenhouse effect, and therefore warming with increased pN<sub>2</sub>. This might suggest cooler climates at low pN<sub>2</sub>, but Zahnle and Buick (2016) noted that low surface pressures would result in less effective trapping of water vapor in the lower atmosphere, as the tropopause is warmer with low surface pressures (Wordsworth and Pierrehumbert, 2014)—increased stratospheric water vapor would then lead to increased total water vapor and a stronger greenhouse effect, suggesting that climates are warmer at low pN<sub>2</sub> than at higher pressures. Vladilo et al. (2013) included the effects of heat transport, increased heat capacity, and pressure broadening in an ensemble of one-dimensional energy-balance models, and found that the habitable zone appeared broader at high pressures, due primarily to warming at low insolation and reduced water loss at high insolation. However, they increased pCO<sub>2</sub> proportionally with pN<sub>2</sub>, making it difficult to disentangle warming from N<sub>2</sub> and warming from CO<sub>2</sub>. Chemke and Kaspi (2017) modeled a range of surface pressures with a 3D climate model, but did not include pressure broadening or Rayleigh scattering, examining only the dynamical effects. Most recently, Komacek and Abbot (2019) presented the results of five models computed using ExoCAM, a fully-coupled three-dimensional climate model, with surface pressures ranging from 0.25 to 4 bars. They found a nonlinear response, with warming up to 1 bar, and dramatic cooling at 2 and 4 bars, which they attributed to increased Rayleigh scattering. However, their models did not include CO<sub>2</sub>, and they note significant disagreement with previous studies (Goldblatt et al., 2009; Li et al., 2009; Charnay et al., 2013; Wolf and Toon, 2014; Chemke et al., 2016) that suggested increased pN<sub>2</sub> should cause warming through pressure broadening.

Determining the effect of different N<sub>2</sub> partial pressures on the climate is of particular importance for understanding the climate evolution of Earth itself, particularly in the context of the “Faint Young Sun paradox” (Sagan and Mullen, 1972), as a higher N<sub>2</sub> partial pressure has been proposed as a partial solution (Goldblatt et al., 2009). However, the actual pN<sub>2</sub> during Earth’s early history is a matter of debate. Fossilized raindrops suggest that as late as 2.7 Gya, Earth’s pN<sub>2</sub> was less than half its current levels, and that should not represent a significant change from 3–3.5 Gya (Som et al., 2016). However, Johnson and Goldblatt (2017) showed that there was a secular increase in crustal nitrogen during the Precambrian, suggesting that pN<sub>2</sub> has been decreasing over time, supporting their finding in Johnson and Goldblatt (2015) that the bulk silicate Earth contains several bars of nitrogen. Emplacing that much nitrogen in the mantle at any time after the hot conditions of the Hadean is difficult (Wordsworth, 2016), though Stüeken et al. (2016) argued that biological burial and release could lead to sharper swings in pN<sub>2</sub> than would be permitted by geochemistry alone. A deeper understanding of pN<sub>2</sub>’s effect on the climate would make it easier to use paleoclimate indicators to help constrain the evolution of Earth’s atmosphere, and to use geological indicators of pN<sub>2</sub> to constrain other atmospheric constituents in order to resolve the Faint Young Sun paradox.

In this study, we use PlaSim, a fast 3D climate model, to explore the climates of Earth-sized planets in the habitable zone with pN<sub>2</sub> levels ranging from 0.1 to 10 bars. We vary insolation, synchronicity, presence of land, and initial conditions to demonstrate the range of climates permitted by variations in pN<sub>2</sub>, then perform a series of experiments to thoroughly identify the mechanisms responsible for variations in climate. Finally, we explore the impacts of pN<sub>2</sub> on observations of Earth-like exoplanets.

## 2. Methods

### 2.1. Climate Model

We use PlaSim, a 3D general circulation model (GCM) designed for Earth-like climates (Fraedrich et al., 2005). PlaSim uses a spectral core to solve the primitive fluid equations for pressure, temperature, divergence, vorticity, and water vapor advection. We use the model in its T21 configuration, in which the atmosphere is discretized into 32 latitudes, 64 longitudes, and 10 vertical levels. The atmosphere is coupled to a surface model, which includes a mixed-layer slab ocean, thermodynamic sea ice, and a soil model on land that allows for variable soil moisture, advection

of excess water to continental margins (the model’s river system), and icy or snowy surfaces. PlaSim’s hydrological cycle is relatively complete, including soil storage, runoff, surface evaporation, storage as atmospheric water vapor, cloud formation, deep and shallow convection, and precipitation as either rain or snow, including re-evaporation of falling precipitation as the water passes through warmer layers. Radiation is computed using a three-band model, with two shortwave bands and one longwave bands. Absorption and transmissivity are computed in each band according to absorber abundances, while clouds are responsible for gray scattering based on cloud fraction and liquid water path. Rayleigh scattering is computed only in the bottom layer. Pressure broadening of each absorbing species is included, and PlaSim assumes that the pressure-broadened effective abundance of each species scales linearly with local pressure (Fraedrich et al., 2005), following Sasamori (1968) and Strong and Plass (1950).

## 2.2. Modifications to PlaSim

PlaSim does not natively consider varying surface pressure when computing Rayleigh scattering. The scattering transmittance in the bottom layer is computed as direct and diffuse components with prescribed scattering efficiencies (Fraedrich et al., 2005):

$$T_{\text{direct}} = 1 - \frac{0.219}{1 + 0.816\mu_0} \quad (1)$$

$$T_{\text{diffuse}} = 0.856 \quad (2)$$

where  $\mu_0$  is the cosine of the solar zenith angle. We note that  $T_{\text{diffuse}} = 1 - 0.144$ , and that 0.144 is the actual fit parameter corresponding to PlaSim’s assumed scattering optical depth for diffuse radiation. To adapt this prescription for variable surface pressure, we assume that the scattering optical depth of a column of atmosphere scales mostly linearly with the mass of that column, and therefore surface pressure. According to the Beer-Lambert Law, transmittance is exponentially related to the optical depth  $\tau$  (Ingle and Crouch, 1988):

$$T = \exp(-\tau) \quad (3)$$

Our modified prescription therefore computes the optical depth, scales it by the column mass relative to that on Earth, and then computes the transmittance:

$$T' = \exp \left[ \left( \frac{p_s}{p_{s,\oplus}} \frac{g_{\oplus}}{g} \right) \ln T_0 \right] \quad (4)$$

where  $T_0$  is the prescribed transmittance for Earth (direct or diffuse),  $p_s$  is the surface pressure, and  $g$  is the surface gravity.

We also modified PlaSim’s vertical discretization to accommodate variable surface pressures. PlaSim uses a sigma system of vertical discretization, where the vertical coordinate is dimensionless, and its value at a given level is simply the ratio of the current pressure to the surface pressure, such that a vertical coordinate of 1 indicates the surface, and 0 indicates the top of the atmosphere (Fraedrich et al., 2005). PlaSim computes its vertical levels with a fourth-order polynomial that is mostly linear between 0 and 1:

$$\sigma_{h,k} = \frac{3}{4}\sigma_k + \frac{7}{4}\sigma_k^3 - \frac{3}{2}\sigma_k^4 \quad (5)$$

$$\sigma'_k = \frac{1}{2}(\sigma_{h,k} + \sigma_{h,k-1}) \quad (6)$$

where  $\sigma_k$  is linearly-spaced between 0 and 1,  $\sigma_{h,k}$  is the coordinate of the interface between model layers  $k$  and  $k + 1$ , and  $\sigma'_k$  is the coordinate of layer  $k$ ’s mid-point. This scheme is designed to give slightly higher resolution near the surface and near the tropopause, but because it starts from coordinates evenly-spaced in pressure, increasing the surface pressure results in higher pressures for all model layers. With a surface pressure of 10 bars, this means there is almost 1 bar of atmosphere in the model’s top layer. Particularly in the case of radiative phenomenon which depend on optical depth from the top of the atmosphere, such as ozone absorption and heating, this means important physics

can be lost in the low resolution of the top layer. To mitigate this, we simply rescale the layer interface coordinates so that the top interface always occurs at a prescribed pressure  $p_{\text{top}}$ , or  $p_{\text{top}}/p_s$  in sigma-coordinates. We use 50 mbar for most models, ensuring that the top model layer always spans only the top 50 mbar of the atmosphere. For models with surface pressures less than 1 bar, we linearly scaled this down to 5 mbar at  $p_s = 0.1$  bar.

We found in our testing that the model was not particularly sensitive to the choice of  $p_{\text{top}}$ , though choosing a value too low for a high-pressure model could affect model stability. We also experimented with doubling the vertical resolution to 20 levels, and replacing the vertical discretization scheme entirely with one that was logarithmic in pressure, or linearly-spaced in altitude. Simply using a pinned upper layer had very little effect on our results, and doubling the resolution similarly had little effect. Using a logarithmic scheme resulted in higher peak temperatures in the warmest high-pressure models, but reduced PlaSim’s stability while running and required shorter timesteps. We therefore conclude that our initial approach of simply requiring that the top layer not exceed a certain pressure is sufficient.

To verify the validity of these modifications, we compared PlaSim’s shortwave fluxes to those computed with SBDART (Santa Barbara DISORT Atmospheric Radiative Transfer, [Ricchiuzzi et al., 1998](#)), which computes plane-parallel radiative transfer as a function of wavelength. We used 18 PlaSim models at  $1350 \text{ W m}^{-2}$  in an aquaplanet configuration, with surface pressures ranging from 0.1 to 9 bars. We used a single column of output from each model, representing a single instant in time at an equatorial gridpoint during local noon, and used that column as input to SBDART. We ran SBDART on that atmospheric column, ignoring clouds and absorbers such as ozone and water vapor, computing broadband fluxes at each layer from 250 to 750 nm. We then ran PlaSim’s shortwave radiation model on that same column, making the same assumptions, and compared the outgoing shortwave fluxes at the top of the atmosphere. The results of this comparison are shown in [Figure 1](#). Our modified model agrees with SBDART at the top of the atmosphere to within a few percent even with surface pressures up to 10 bars, but we note it does consistently predict more downwelling flux at the surface. It is possible to reduce this disagreement by adjusting the constants in [Equation 1](#) and [Equation 2](#), but this would change PlaSim’s overall output when applied to the standard Earth climate. PlaSim has been used extensively for Earth-like climates (e.g. [Fraedrich et al., 2005](#); [Boschi et al., 2013](#); [Holden et al., 2016](#); [Nowajewski et al., 2018](#); [D’Errico et al., 2018](#)), and we do not wish to make modifications that would require significant re-tuning and re-validation on the modern Earth climate. We therefore accept the disagreement at the surface, noting its consistency across surface pressure, as a difference in model parameterization, and take the agreement between PlaSim and SBDART in outgoing shortwave flux and therefore total shortwave energy budget as an indication of the validity of our modifications for the present study.

### 2.3. Modeling Strategy

To assess the effect of  $p\text{N}_2$  on the climate, we kept  $p\text{CO}_2$  constant at  $360 \mu\text{bar}$ , and varied  $p\text{N}_2$  from 0.1 to 10 bars, and insolation from  $1100$  to  $1550 \text{ W m}^{-2}$ , computing a grid of 160 models. PlaSim does not differentiate between background gases such as  $\text{O}_2$  and  $\text{N}_2$ , so here we assume that the entirety of the atmosphere’s background gas fraction is  $\text{N}_2$ , and vary  $p\text{N}_2$  alone by increasing the surface pressure while reducing the  $\text{CO}_2$  concentration. Since here we define a ‘background gas’ as having negligible contribution to the energy budget through visible or infrared absorption or emission lines, we do not expect the choice of a different background gas to have much impact on our results beyond changing the atmosphere’s mean molecular weight, with the notable exception that  $\text{H}_2$ -dominated atmospheres are likely to behave very differently due to having a larger thermal scale height than a steam atmosphere ([Koll and Cronin, 2019](#)). To isolate the dynamical effects of surface pressure and the radiative effects of  $\text{N}_2$ , we assume a fixed background gas mean molecular weight identical to that in Earth’s atmosphere. We run each model until both the surface and top of the atmosphere have reached a stable energy balance, which typically involves 75–200 years of model time. We run PlaSim on 16-core nodes on our local computing cluster, which takes approximately 45 seconds per model year. We assume Earth’s modern continental distribution and topography for each model in this grid, but we also perform several experiments with aquaplanet configurations (no land; sea surface everywhere) to simplify the model and rule out the role of land surface processes. We assume that the ocean mixed layer thickness is 50 meters in all our models.

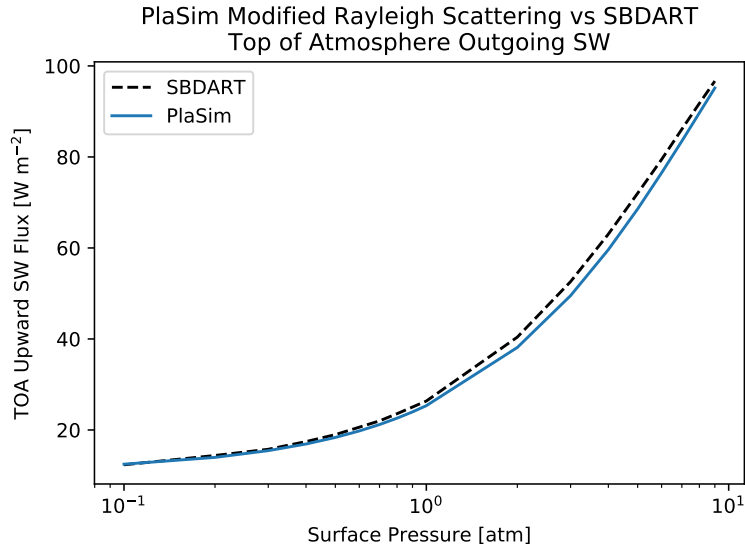


Figure 1: Comparison of shortwave fluxes computed using SBDART and PlaSim’s shortwave model with our modified Rayleigh scattering and vertical discretization. We ignore clouds and absorbers such as ozone and water vapor. This comparison uses as input a column of PlaSim output at a single instant in time at an equatorial gridpoint from equilibrated PlaSim models at  $1350 \text{ W m}^{-2}$ , spanning surface pressures of 0.1–9 bars. Our modified PlaSim radiation model shows good agreement with SBDART at the top of the atmosphere for a range of surface pressures.

### 3. Results

As shown in Figure 2, we find that the effect of increasing  $p\text{N}_2$  on global temperatures is nonlinear: at low pressures, increasing  $p\text{N}_2$  results in warmer average temperatures, while at higher pressures, increased  $p\text{N}_2$  can cool the climate, resulting eventually in a transition to a snowball state, where sea ice extends all the way to the equator (Pierrehumbert, 2005). For planets in snowball states, we find increasing  $p\text{N}_2$  results in monotonic cooling, rather than the warming trend seen on temperate planets, as shown in the right side of the bottom left plot in Figure 2. The warming associated with  $p\text{N}_2$  is significant; planets with 4 or 5 bars of  $\text{N}_2$  can be an average of almost 40 K warmer than planets with 1 bar. We further find that the  $\text{N}_2$  partial pressure at which average surface temperatures reach their maximum varies as a function of insolation, such that the  $p\text{N}_2$  required to begin cooling the planet is higher at high insulations than at low insulations. Maximum and mean surface temperatures in some parts of the parameter space are high enough to potentially indicate a transition to a runaway greenhouse. While PlaSim has been used before to study this transition (Gomez-Leal et al., 2019), we have not validated PlaSim’s performance in both high-temperature and high-pressure regimes, and therefore refrain from concluding that these models represent the inner edge of the habitable zone. We note however that the observed trends do suggest that the inner edge may move to lower insulations for intermediate surface pressures, and recommend further study.

We note that a similar nonlinear sensitivity to  $p\text{N}_2$  was observed in ExoCAM models reported in Komacek and Abbot (2019), but their results included a limited number of models and had no  $\text{CO}_2$ , making it difficult to draw conclusions about the mechanisms responsible for the trend from their models alone. The fact that the same qualitative behavior appears in both GCMs however suggests that this is not model-dependent behavior, and instead representative of underlying physics.

Vladilo et al. (2013) argued that the width of the habitable zone should increase with increasing  $p\text{N}_2$ , using results from a 1D EBM. We find however that the width of the habitable zone is likely to decrease at high pressures. We note two important differences between our work and theirs: Vladilo et al. (2013) assumed constant mixing ratios for non-condensable greenhouse gases such as  $\text{CO}_2$ , such that the non-water greenhouse effect always increases with pressure (beyond that expected from pressure broadening), and their EBM did not include Rayleigh scattering as a source of higher albedo at high pressures, although it did include horizontal heat transport. While we do not attempt to calculate the actual edges of the habitable zone as described in Kopparapu et al. (2013), we note that the climate’s sensitivity to

## Fast-Rotating Climates with Varying $pN_2$

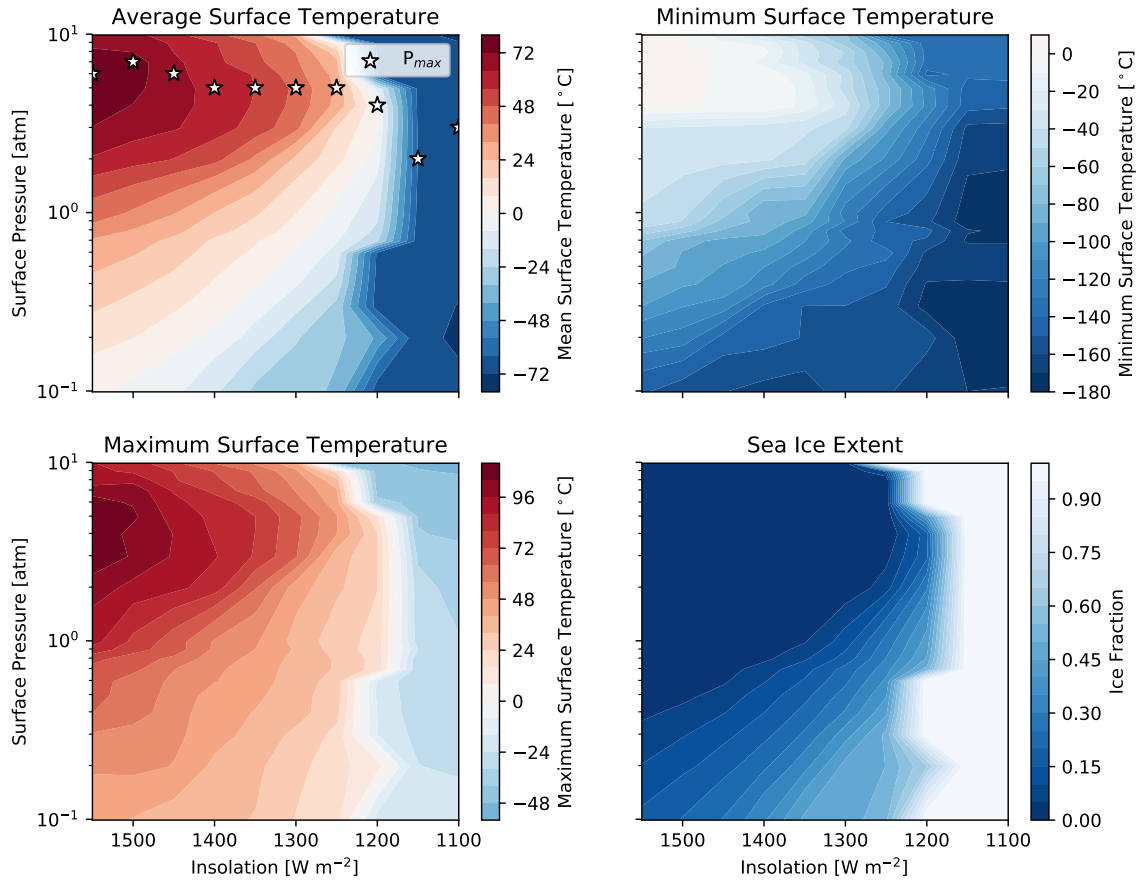


Figure 2: Mean, minimum, and maximum surface temperatures, along with sea ice extent, for a grid of 160 PlaSim models of Earth-like planets with varying surface pressures. In varying surface pressure, we only varied the Nitrogen partial pressure ( $pN_2$ )— $pCO_2$  was held constant. The climate demonstrates nonlinear sensitivity to the amount of background gas, showing significant warming in some regimes and significant cooling in others. This is due to warming by pressure broadening, cooling by Rayleigh scattering, and cooling by heat transport all competing with each other. The stars labeled  $P_{max}$  in the upper-left panel indicate the surface pressures at which the mean temperature is maximized. We note that while temperatures likely exceed the greenhouse runaway limit in some regions of the parameter space, we have not evaluated PlaSim’s performance at that transition and therefore cannot conclusively say that high  $pN_2$  could lead to a runaway greenhouse.

Experiment	Warming	Cooling
No Rayleigh Scattering	Yes	<b>No</b>
No Advection	Yes	Yes
No Sea-Ice Feedback	Yes	Yes
No Clouds	Yes	Yes
No Oceans; Wet Soil	Yes	Yes
No Water Vapor	<b>No</b>	Yes
No Water Vapor; No Advection	<b>No</b>	Yes
No Water Vapor; No Rayleigh Scattering	<b>No</b>	Yes
No Advection; No Water Vapor; No Scattering	Yes	<b>No</b>
No Pressure Broadening	<b>No</b>	Yes
No Advection; No H <sub>2</sub> O; No Scattering; No Broadening	<b>No</b>	Yes
No Advection; No H <sub>2</sub> O; No Scattering; No CO <sub>2</sub>	<b>No</b>	<b>No</b>

Table 1: Experiments performed to identify the cause of warming with **increased** pN<sub>2</sub>. In each experiment, we varied pN<sub>2</sub> from 1 to 10 bars. Results are bolded where the outcome differs from the behavior found in Figure 2. These results suggest that the dominant cooling mechanism is increased Rayleigh scattering, and the dominant warming mechanism is warming by pressure broadening, amplified by the water vapor greenhouse positive feedback. Without water vapor, pressure-broadening is not a sufficiently-large effect to counter the effects of scattering and heat transport. Increased heat transport cools the climate, but in these experiments was insufficient to counter water-amplified warming alone, in contrast to Rayleigh scattering, which was sufficient.

insolation is higher at high pressures, resulting in a faster decrease in average temperatures with increasing distance from the Sun. This suggests that with increasing pressure the inner edge should move outwards, while the outer edge moves inwards. A possible explanation for this observation is that in the limit of very efficient heat transport, as is found at high pressures, surface temperature gradients are small. A consequence of this fact is that as insolation or greenhouse forcing changes, the climate is less able to buffer the change in energy budget by moving excess heat away from strongly-irradiated regions or replacing heat lost in cool regions. Additionally, a small horizontal temperature gradient means a small decrease in average temperature results in a large amount of ocean surface falling below the freezing point, so the transition from ice-free to snowball is sharper.

## 4. Discussion

### 4.1. Mechanisms of Action on the Climate

Cooling from increased N<sub>2</sub> was expected (Nakajima et al., 1992; Komacek and Abbot, 2019), because increased Rayleigh scattering should increase the top-of-atmosphere albedo, increased heat transport efficiency should mean more efficient heat loss to space, and a drier lapse rate should lead to more efficient cooling of the surface and lower atmosphere. However, because N<sub>2</sub> lacks absorption lines in the thermal infrared, increasing pN<sub>2</sub> was not expected to cause significant warming in our models. To investigate the cause of our observed warming trends, we conducted a number of experiments in which model components were selectively removed. In experiments in which water vapor was removed, we increased the effective solar constant to offset the loss of the water vapor greenhouse, assuming a surface temperature of 280 K for a 1 bar atmosphere, such that  $T_{\text{eff}} = [I_0(1 - \alpha)/(4\sigma)]^{1/4}$ , where  $I_0$  is the insolation,  $\alpha$  is albedo, and  $\sigma$  is the Stefan-Boltzmann constant. A summary of our experiments and their outcomes is given in Table 1.

The primary contribution to cooling at higher pN<sub>2</sub> in our experiments was the reduction in net shortwave heating due to increased reflection by Rayleigh scattering. Poleward heat transport does contribute to cooling on planets with Earth-like rotation, but to a lesser extent—its impact on global average temperatures is only apparent when the other major heating and cooling mechanisms are removed. We found that the warming trend in Figure 2 could only be reversed by eliminating the water vapor greenhouse effect, either by removing water vapor entirely or by removing pressure broadening. Without heat transport or Rayleigh scattering, the global average temperature increases monotonically with increasing pN<sub>2</sub>, until moist runaway conditions are reached. The initial heating amplified by the water vapor greenhouse comes from pressure broadening of the CO<sub>2</sub> and H<sub>2</sub>O absorption bands. The effect of pressure broadening on its own, however is small—no more than 5–10 K between 1 and 10 bars of pN<sub>2</sub>. In experiments with

cooling mechanisms such as Rayleigh scattering or heat transport enabled, the heating effect from pressure broadening is sufficiently weak for the overall trend to be colder temperatures with increased  $pN_2$ —amplification from the water vapor positive feedback is necessary for pressure-broadening to be the dominant mechanism. In the absence of water vapor, heat transport, scattering, or pressure broadening, a slight cooling trend remains—approximately 0.5 K over 1–10 bars. This cooling trend disappears when  $CO_2$  is removed as well, suggesting that the vertical distribution of  $CO_2$  in taller atmospheres is very slightly more efficient at cooling the surface. The amount of warming we find from the inclusion of water vapor is probably slightly underestimated, since the amount and altitude of stratospheric warming by ozone is prescribed in PlaSim. In reality, because ozone’s major radiative contribution is absorption of ultraviolet incident light, peak absorption should generally occur around the same pressure level, resulting in ozone absorption occurring at higher altitudes on planets with thicker atmospheres (Wilcox et al., 2012). This should in turn result in a higher and colder tropopause (Wordsworth and Pierrehumbert, 2014), allowing a larger volume of water vapor to mix into the troposphere, thus strengthening the water vapor greenhouse effect at higher  $pN_2$ .

The relationship between these different mechanisms is very apparent when considering the difference between temperate Earth-like planets and snowball planets, where the surface is entirely covered by sea ice (Pierrehumbert, 2005). Due to the high albedo of sea ice, this state is bistable with temperate, mostly ice-free climates across a range of insulations and  $CO_2$  levels (Budyko, 1969; Sellers, 1969). We examined the response of both temperate and snowball climates to differences in  $pN_2$ , as shown in Figure 3, corresponding to a slice through the grid in Figure 2 at  $1300 \text{ W m}^{-2}$  for both warm- and cold-starts. The temperate models display the strong, nonlinear response shown in Figure 2, with increased heating through pressure broadening amplified by abundant atmospheric water vapor, and eventual cooling by Rayleigh scattering. On the other hand, the snowball models appear much less sensitive to  $pN_2$ , varying by only 4 K over 10 bars, despite the inclusion of the water vapor greenhouse effect. This low sensitivity is the result of cold temperatures and sea ice imposing limits on evaporation rates, thus limiting the strength of the water vapor positive feedback. The snowball models also appear less sensitive to cooling by Rayleigh scattering because the planet’s overall albedo is already very high, due to the highly-reflective surface. An increase in atmospheric albedo can therefore do little to raise the overall albedo, resulting in much smaller changes to the planet’s energy budget, as shown in Figure 4. In other words, the additional scattered light on a snowball planet is mostly light that would have been reflected anyway, as opposed to a temperate planet or a dry desert planet with a dark surface where that light would have been mostly absorbed. The importance of surface albedo in determining the climate’s sensitivity to  $pN_2$  suggests that any planet with a dark surface, i.e. planets without extensive ice or snow cover, will undergo strong cooling from increased Rayleigh scattering at high  $pN_2$ . Land planets which are not completely dry, such as those in Abe et al. (2011), would exhibit strong cooling from Rayleigh scattering even at snowball-like temperatures, so long as the available water vapor did not produce extensive snow cover.

These results suggest that the effects of changing  $pN_2$  can be largely segregated into three different regimes:

1. **High  $pN_2$ :** Rayleigh scattering dominates, and adding  $pN_2$  cools the climate.
2. **Wet Surface:** A large surface water reservoir permits strong evaporation at low  $pN_2$ . The water vapor greenhouse effect dominates due to pressure broadening, and adding  $pN_2$  warms the climate.
3. **Dry Surface:** Atmospheric water vapor is limited by low evaporation. Rayleigh scattering and heat transport are the dominant effects, and increasing  $pN_2$  monotonically cools the climate, even at low  $pN_2$ .

Therefore on planets with a limited water vapor greenhouse, either due to evaporation limited by sea ice or an overall lack of surface water, increasing  $pN_2$  results in colder climates, while the opposite effect is found on planets with large surface water inventories and enough insolation to drive large amounts of evaporation. At sufficiently high  $pN_2$ , other details of the climate matter less, as Rayleigh scattering is strong enough to cause cooling regardless of the planet’s water inventory. We do not expect a more-realistic layer-by-layer treatment of Rayleigh scattering in PlaSim to change this conclusion, as scattering in a high- $pN_2$  atmosphere would simply occur above where water absorption would occur.

#### 4.2. $pN_2$ on Tidally-locked Planets

On planets with Earth-like rotation rates, heat transport is rarely the dominant effect of  $pN_2$ , as Rayleigh scattering and pressure broadening of trace absorbers both have much stronger impacts on the climate. However, heat transport has a much larger climatic effect on tidally-locked and slow-rotating planets. On these planets, the interplay between

### Temperate vs Snowball Response to $pN_2$

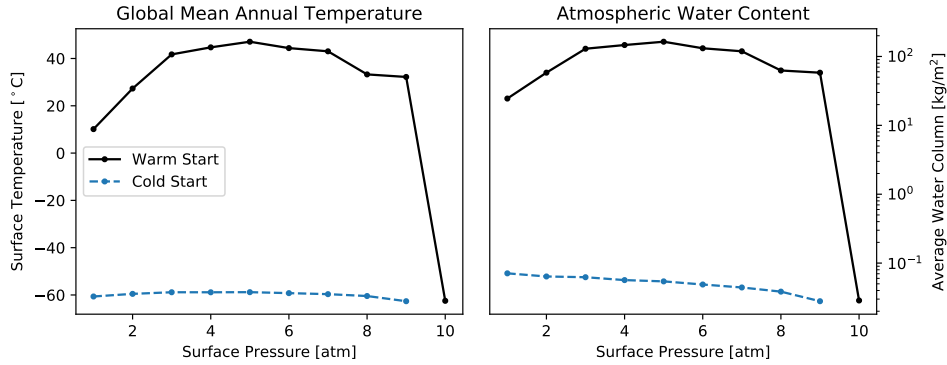


Figure 3: Global mean annual surface temperature and average water column for varying surface pressures, in both warm-start and cold-start (snowball) scenarios. In our cold-start scenarios, the ocean surface is entirely covered in sea ice. Warm-start models display the strongly nonlinear response identified in Figure 2, while snowball models do not. The relatively large availability of water vapor in the temperate models means that pressure broadening of the  $CO_2$  and water vapor absorption lines causes a large amount of warming, such that temperatures only decrease with a large amount of Rayleigh scattering at high surface pressures. On snowball planets, however, the limited availability of water vapor results in pressure broadening causing a small amount of warming at lower surface pressures, but Rayleigh scattering and heat transport quickly dominate, resulting in monotonically-decreasing water vapor abundance. In general, snowball planets are less sensitive to changes in  $pN_2$ , because the high surface albedo limits the degree to which atmospheric scattering can affect the overall albedo.

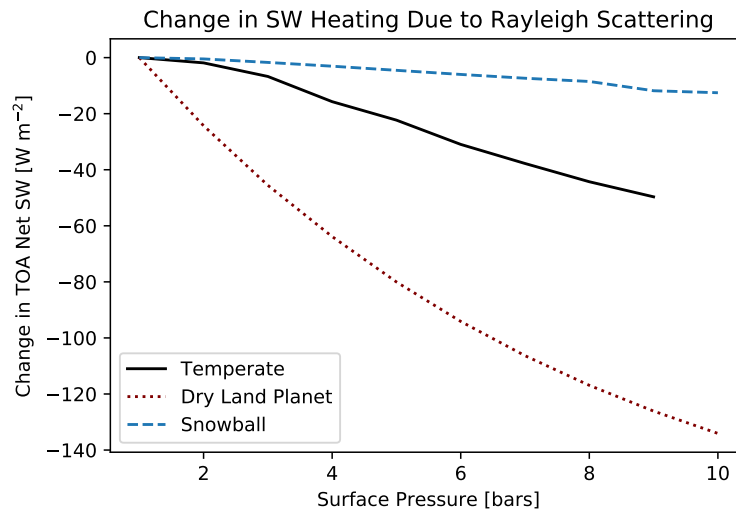


Figure 4: Change in shortwave heating due to increased Rayleigh scattering, for temperate and snowball planets at  $1300 W m^{-2}$  and dry land planets at  $2000 W m^{-2}$  with  $360 \mu\text{bars}$  of  $CO_2$ . The land planets have uniform gray soil albedos of 0.1. The increase in light reflecting off the atmosphere should be the same for all climates (ignoring cloud effects), but the climate sensitivity of snowball planets to Rayleigh scattering is quite a bit lower than that of either temperate or dry land planets with low soil albedos. This is because the overall top-of-atmosphere albedo of a snowball planet is already high, so an increase in reflection from atmospheric scattering primarily reduces how much light would be reflected off the surface, rather than primarily reducing how much light would be absorbed. This results in a smaller change to the energy budget as measured by net shortwave flux at the top of the atmosphere.

## Tidally-Locked Climates with Varying $pN_2$

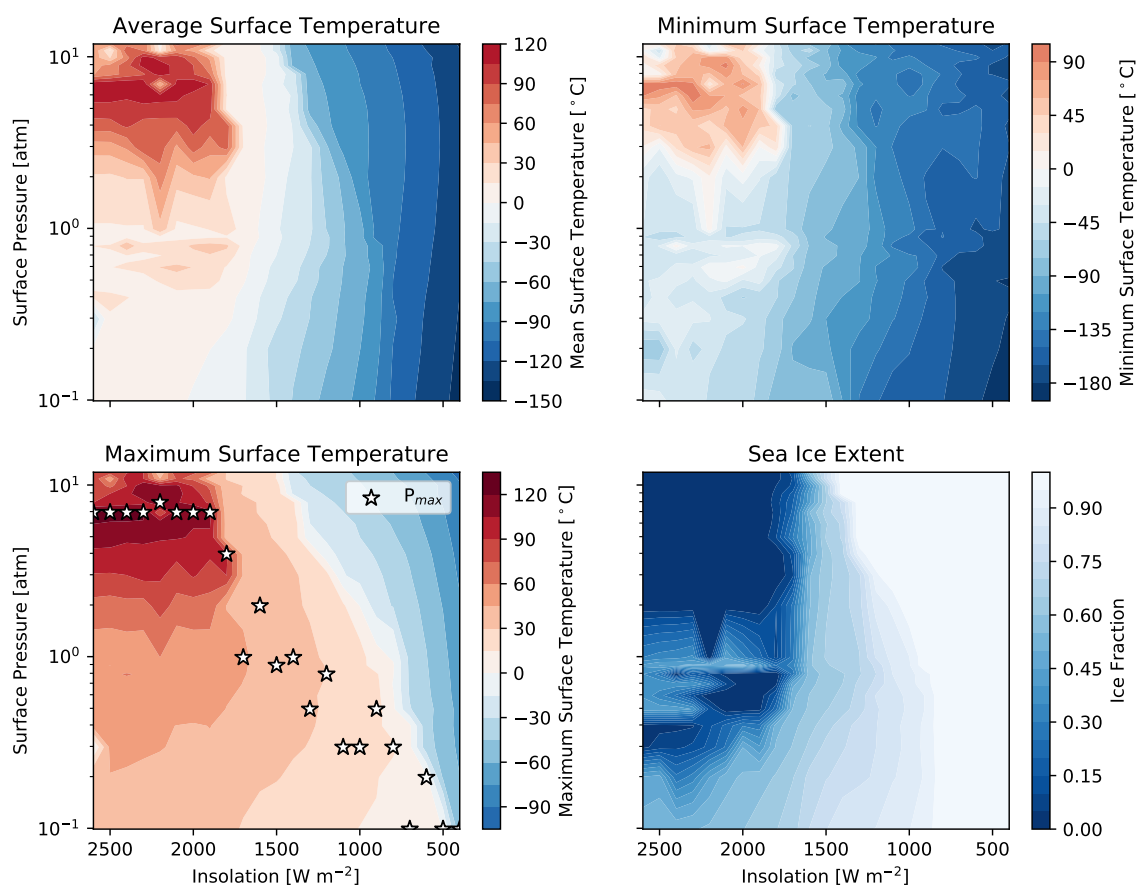


Figure 5: Mean, minimum, and maximum surface temperatures, along with sea ice extent, for a grid of 483 PlaSim models of tidally-locked planets with varying surface pressures. As in Figure 2, the stars labeled  $P_{max}$  in the bottom-left panel indicate the pressure at which the maximum temperature peaks. Only  $pN_2$  was varied— $pCO_2$  was held constant. In contrast to Figure 2, on tidally-locked planets  $pN_2$  primarily cools the climate at lower insulations, while at higher insulations we see the same nonlinear behavior resulting from competing warming and cooling mechanisms as on Earth-like planets. This difference is because heat transport is much more important on tidally-locked planets, where advection of heat onto the night-side is a major component of the planet’s total energy budget. There appears to be complex structure at high insulations, but as these climates are on the extreme end of what PlaSim can model, more work is required to determine its significance.

these three mechanisms may be more complex. To investigate this, we computed a grid of 483 models with PlaSim in a tidally-locked configuration, with insolations ranging from 400 to 2600 W m<sup>-2</sup> and surface pressures ranging from 0.1 to 12 bars. For simplicity, each model was in an aquaplanet surface configuration. PlaSim has been used before to study tidally-locked planets (Menou, 2013; Checlair et al., 2017; Abbot et al., 2018), but we introduced small modifications to ensure that numerical hyper-diffusion timescales would use 24-hour days for unit conversions between days and seconds, rather than simply using the current length of the solar day (which is properly undefined for a tidally-locked planet). While most tidally-locked habitable zone planets orbit low-mass stars with much redder spectra than the Sun, here we assume a solar-like input spectrum. We do not include the effects of a different input spectrum because we wish to isolate the ways in which the geometry and dynamics of tidally-locked planets affect the relative strengths of the mechanisms of action we identified in subsection 4.1. Further work will be required to investigate how a redder spectrum affects the climate’s sensitivity to pN<sub>2</sub>. The minimum, mean, and maximum temperatures of our tidally-locked models, along with sea ice fraction, are shown in Figure 5.

On these planets, the climate is very sensitive to the efficiency with which heat can be advected from the dayside to the night side (Checlair et al., 2017; Haqq-Misra et al., 2018). As pN<sub>2</sub> increases, heat transport efficiency increases, resulting in significant cooling. Combined with increased Rayleigh scattering, warming by pressure broadening only dominates at low pN<sub>2</sub> where heat transport and scattering are weak, and at high insolations where there is high potential for surface evaporation, resulting in very strong amplification through the water vapor greenhouse. The consequence of this difference between high and low insolations is that the surface pressure at which dayside surface temperatures are maximized moves to lower pressures as insolation decreases, as shown in Figure 5. This is consistent with our findings in Figure 2, where we found a similar trend on planets with Earth-like rotation. Here we are using changes in maximum temperature as the metric for the impact on the climate, in contrast to the average surface temperature, which we used in section 3. This is because the geometry of tidally-locked climates and the importance of horizontal heat transport on these planets means that changes in the global average surface temperature may not be particularly indicative of trends in the dayside climate. Our finding in section 3 that the habitable zone likely narrows at higher surface pressures seems to hold here as well, with a sharper transition at high pressures from hot to frozen climates than at low surface pressures. In general, we find that the increased importance of heat transport on tidally-locked planets results in increasing pN<sub>2</sub> causing cooling in more of the parameter space than on fast-rotating Earth-like planets at the same pressures and insolations. More work however is necessary to explore the effects of different N<sub>2</sub> partial pressures on the tidally-locked habitable zone, particularly with a redder input spectrum.

#### 4.3. Impact of pN<sub>2</sub> on Observables

Our findings in section 3 and subsection 4.2 suggest that Earth-like climates are highly-sensitive to the amount of background gases present in the atmosphere. However, in the case of N<sub>2</sub>, the absence of absorption lines in the visible or infrared makes it difficult to quantify the abundance of background gases on terrestrial planets with transit spectroscopy (Benneke and Seager, 2012). Even if the Rayleigh scattering slope as a function of wavelength could be observed in transit spectroscopy, the presence of a cloud deck could limit efforts to constrain the total thickness of an atmosphere (Kaltenegger et al., 2007; Benneke and Seager, 2012; Barstow et al., 2016). Observations using reflected light can more-easily probe deeper into the atmosphere (e.g. Snellen et al., 2015), so we investigated the possibility that pN<sub>2</sub> might have observable signatures in reflected light.

We used the radiative transfer package SBDART (Ricchiazzi et al., 1998) to compute reflectance and emission spectra for our models. Spatially-resolved images of exoplanets are not currently possible, so to compute the disk-averaged spectrum of each model, we run SBDART on each column of the model’s output that would be visible to an observer for a given snapshot in time, using PlaSim’s output to specify water abundances, cloud fractions, surface type, and air temperature, and specifying the solar zenith angle and observer’s viewing angle according to the latitude and longitude of each model column. In most of our models we assume the observer and Sun are both in the same place in the sky over the planet (corresponding to a planet as seen in secondary eclipse). In addition to this equatorial-view geometry, for our tidally-locked models we also compute spectra for a polar-view geometry, where the system is face-on relative to the viewer, such that only half of the viewer-facing hemisphere is illuminated. We use the MODTRAN-3 input solar spectrum, which has a resolution of 20 cm<sup>-1</sup>. We assume a solar input spectrum for both Earth-like and tidally-locked models for consistency with PlaSim and to isolate the effect of changing pN<sub>2</sub> from that of changing the input spectrum. Because Rayleigh scattering is responsible for the sky’s distinctive blue color, the effect of increased Rayleigh scattering from higher pN<sub>2</sub> should be apparent in broadband photometry. We

## Planetary Color as a Function of $pN_2$

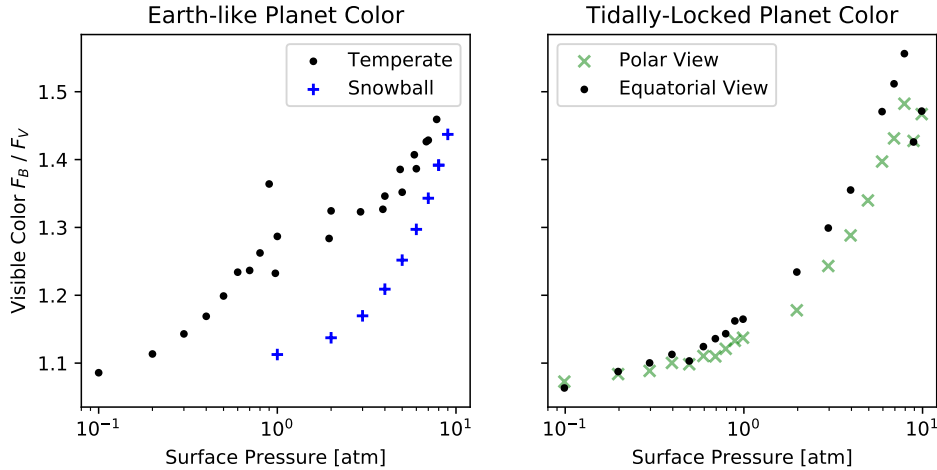


Figure 6: B–V photometric colors of Earth-like and tidally-locked planets in reflected light. The Earth-like models (assuming 24-hour rotation) are all computed assuming equatorial, zenith viewing geometries consistent with the planet being in secondary eclipse. Both equatorial and polar viewing geometries are shown for the tidally-locked planets. These fluxes were computed by running SBDART on each column of PlaSim model output. The Earth-like models include both aquaplanet and Earth-like land configurations together with warm- and cold-starts, while the tidally-locked planets are pure aquaplanets. The Earth-like models are computed at an insolation of  $1350 \text{ W m}^{-2}$  and the tidally-locked models are at  $1400 \text{ W m}^{-2}$ . We find that across terrestrial planet types, planets with higher  $pN_2$  are consistently bluer due to increased Rayleigh scattering.

therefore integrate the resulting high-resolution spectra across B and V bands,  $445 \pm 47$  and  $551 \pm 44$  nm (Binney and Merrifield, 1998), assuming flat box-like filter response functions with 100% transmittance.

We did not compute spectra for every single model reported in this study, as our aim is not to solve the inverse problem in a way that permits robust retrieval of  $pN_2$  for any terrestrial habitable zone exoplanet, but rather to identify the impact of  $pN_2$  on potential observables. Factors such as cloud coverage, sea ice extent, photochemistry, and the colors of different surface rocks will all likely be sources of confusion in efforts to robustly and uniquely retrieve  $pN_2$ . We computed spectra for planets lacking any land (aquaplanets) and with modern Earth continents (with Africa centered beneath the observer) at  $1350 \text{ W m}^{-2}$ , as well as cold-start “snowball” versions of both surface configurations, varying  $pN_2$  from 0.1 to 10 bars for each type of planet. Snowball models that had land had land surfaces almost entirely covered in snow. Tidally-locked planets do not undergo snowball bifurcations in the way that Earth-like planets do (Checlair et al., 2017), so we cannot perform a similar comparison for those planets. However, tidally-locked planets may appear mostly ice-covered when their systems are observed face-on. Direct imaging campaigns may favor systems with polar viewing geometries due to the potential for longer continuous integration times, and tidally-locked planets at moderate insolations typically have sea ice fractions above 0.5 due to the cold night-side, with open ocean only found near the center of the day-side (Pierrehumbert, 2011; Heng and Vogt, 2011; Yang et al., 2013, 2014). Combined with projection effects reducing the apparent size of unfrozen areas near the limb of the visible disk, this results in mostly-frozen observer-facing hemispheres. Therefore for our tidally-locked models, we only compute spectra for a slice at  $1400 \text{ W m}^{-2}$  (to capture a range of sea ice fractions) and instead of warm- and cold-start models, consider equatorial and polar viewing geometries for a single set of models.

The B–V colors of each group of models are shown in Figure 6. Increasing  $pN_2$  results in stronger reflectance at short wavelengths compared to longer wavelengths, resulting in bluer planets. Very strong reflectance by surface ice seems to partially counteract this, potentially because scattering works in both directions, such that while incident blue light is more likely to scatter off the atmosphere back into space and therefore less likely to reach the ground, blue light reflecting off the surface is also more likely to scatter off the atmosphere and therefore less likely to reach space. Put another way, the component of reflected light reaching the observer that is reflecting off the atmosphere itself is preferentially blue, but the component that is reflecting off the surface is preferentially red. Because surface ice is

much more reflective than land or ocean, snowball planets therefore appear less blue. Once  $pN_2$  is sufficiently high, however, the atmosphere becomes optically-thick to Rayleigh scattering, surface information is obscured, and both temperate and snowball planets appear similarly blue. We observe a similar effect on the B–V color of tidally-locked planets. The similarity in observable trends observed across both Earth-like and tidally-locked models allows us to identify  $pN_2$  as the direct cause of the change in observables, rather than a climatic effect such as a change in cloud cover.

#### 4.4. Caveats

While we believe our results are robust due to agreement with ExoCAM (Komacek and Abbot, 2019) and consistency across a diversity of climates, there are nonetheless a number of model caveats that make any quantitative predictions of specific climates suspect. Perhaps most importantly, PlaSim’s implementation of Rayleigh scattering assumes that all scattering happens at the atmosphere’s bottom layer, which is not physically realistic. The impact on the climate’s energy budget for Earth-like surface pressures and lower is negligible, as the atmosphere’s exponential density profile means most scattering does indeed happen in the lower layers of the atmosphere, below cloud tops, and absorption by the surface is the primary way visible light enters the climate’s energy budget (Pierrehumbert, 2010). However, at higher surface pressures, scattering at higher levels of the atmosphere may become important. In models more realistic than PlaSim, atmospheric absorption of visible and near-infrared light by water vapor and oxygen also contributes to the climate’s energy budget (e.g. Way et al., 2017), and scattering in the middle and upper atmosphere may affect that.

In addition to shortcomings in the scattering parameterization, PlaSim’s ozone abundance is prescribed as a normal distribution peaked at 20 km above the surface. This may be appropriate for Earth’s atmosphere, but in an atmosphere where  $N_2$  and  $O_2$  are well-mixed, the height of peak ozone production will depend on the UV optical depth from the top of the atmosphere, resulting in higher-altitude ozone with higher surface pressures (Wilcox et al., 2012). This should have a large effect on the stratospheric heating profile, possibly resulting in a higher and colder tropopause (Wordsworth and Pierrehumbert, 2014). That may allow for a larger water column and thus additional heating, but more work is needed to assess the effect of ozone layer altitude.

As mentioned in subsection 4.3, we have also not considered the role that photochemistry, hazes, aerosols, and differences in cloud formation efficiency might play in thick  $N_2$  atmospheres. In addition to affecting observables, these factors would likely also affect the climate’s energy budget (Arney et al., 2017; Chen et al., 2018, 2019). Most of these factors are not feasible to study fully with PlaSim, and so would require further work with a more sophisticated model.

Finally, we have assumed a solar-like input spectrum in all of our models. One of the major mechanisms by which  $N_2$  affects the climate is Rayleigh scattering, which is most efficient at short wavelengths (Rybicki and Lightman, 2004). Earth-like planets around lower-mass stars would instead receive most of their light at red and infrared wavelengths, meaning Rayleigh scattering’s contribution to the climate’s energy budget would be lessened considerably. In these climates, we can likely expect cooling through heat transport and warming through pressure broadening to be the dominant ways that  $N_2$  affects the climate, as the reduced importance of Rayleigh scattering at high  $pN_2$  will reduce the impact of  $pN_2$  on shortwave heating.

## 5. Conclusion

We have used a large ensemble of GCMs in which  $pN_2$  was varied for a range of insolation and initial conditions, for both Earth-like and tidally-locked rotation, and for both aquaplanet and modern Earth land distributions. We found that the climate’s response to  $pN_2$  is strong and nonlinear, with increasing  $pN_2$  leading to warming in some regimes, and cooling in others. We performed a number of experiments to isolate the mechanisms responsible, and conclude that at low and moderate surface pressures on planets with large surface water reservoirs for evaporation, pressure broadening of the  $CO_2$  and  $H_2O$  absorption lines leads to significant heating. At high surface pressures and in dry climates, Rayleigh scattering dominates over pressure broadening even in the presence of  $CO_2$ , leading to cooling. On planets with very efficient cooling through horizontal heat transport, such as tidally-locked planets, increased heat transport at high surface pressures further leads to cooling, reducing the potential of pressure broadening to cause net warming. Our results are consistent with those reported in Komacek and Abbot (2019), and demonstrate

the relationship between the various seemingly-contradictory mechanisms explored and reported in Nakajima et al. (1992); Goldblatt et al. (2009); Zahnle and Buick (2016); Chemke and Kaspi (2017), and Komacek and Abbot (2019). Finally, we showed that, while  $pN_2$  may be difficult to quantify with transit spectroscopy, high  $pN_2$  will result in planets appearing ‘bluer’ in reflected light, which may be detectable with broadband reflected light photometry.

The history of Earth’s  $pN_2$  is poorly-constrained (Olson et al., 2018), and we have little to no constraints on likely  $N_2$  partial pressures on terrestrial exoplanets, particularly those with formation histories and stellar environments different from our own. Even within our own solar system,  $pN_2$  varies between terrestrial planets with atmospheres—Venus has over 3 bars of  $N_2$  in its atmosphere (Oyama et al., 1980). Our results show however that  $pN_2$  is a crucial ingredient in assessing a planet’s climate and habitability. We have determined that  $pN_2$  will have an impact on observables accessible through direct imaging and secondary eclipse spectroscopy, but more work is needed to understand its role and evolution on planets with both Earth-like and non-Earth-like geophysical and geochemical properties. Furthermore, while increased  $pN_2$  has been proposed as a possible resolution to the ‘faint young Sun paradox’ (Johnson and Goldblatt, 2017), in our sample increased  $pN_2$  alone is not able to sufficiently warm an Earth-like planet at Archaean Earth insolation. We have not however fully-explored the parameter space of atmospheric compositions that may have accompanied increased  $pN_2$ . Theoretical studies of potential climate and habitability of specific exoplanets should therefore include a variety of background gas partial pressures and compositions when assessing the end-members of possible climate scenarios.

## 6. Acknowledgments

AP is supported by the Department of Astronomy & Astrophysics at the University of Toronto, BLF is supported by the Department of Physics at the University of Toronto, KM is supported by the Natural Sciences and Engineering Research Council of Canada, and CL is supported by the Department of Physics at the University of Toronto. Computing resources were provided by the Canadian Institute for Theoretical Astrophysics at the University of Toronto. The authors would like to thank Dorian Abbot for suggestions of existing literature on the role of  $pN_2$  in the climate, and the attendees of the Comparative Climatology of Terrestrial Planets III conference in Houston, Texas in August 2018 for an enlightening and thought-provoking discussion about the difficulties in reconstructing the early Earth’s  $pN_2$  history and evolution. The modified version of PlaSim used in this study is available on AP’s github (Paradise et al., 2019).

We would furthermore like to acknowledge that our work was performed on land traditionally inhabited by the Wendat, the Anishnaabeg, Haudenosaunee, Métis, and the Mississaugas of the Credit First Nation.

- Abbot, D. S., Bloch-Johnson, J., Checlair, J., Farahat, N. X., Graham, R. J., Plotkin, D., Popovic, P., Spaulding-Astudillo, F., feb 2018. Decrease in Hysteresis of Planetary Climate for Planets with Long Solar Days. *The Astrophysical Journal* 854 (1), 3.  
 URL <http://arxiv.org/abs/1801.10551><http://dx.doi.org/10.3847/1538-4357/aaa70f><http://stacks.iop.org/0004-637X/854/i=1/a=3?key=crossref.e0325e68e507678dff38fffd59736583>
- Abe, Y., Abe-Ouchi, A., Sleep, N. H., Zahnle, K. J., 2011. Habitable zone limits for dry planets. *Astrobiology* 11 (5), 443–460.
- Arney, G. N., Meadows, V. S., Domagal-Goldman, S. D., Deming, D., Robinson, T. D., Tovar, G., Wolf, E. T., Schwieterman, E., 2017. Pale Orange Dots: The Impact of Organic Haze on the Habitability and Detectability of Earthlike Exoplanets. *The Astrophysical Journal* 836 (1), 49.  
 URL <http://arxiv.org/abs/1702.02994>
- Barstow, J. K., Aigrain, S., Irwin, P. G., Kendrew, S., Fletcher, L. N., 2016. Telling twins apart: Exo-Earths and Venuses with transit spectroscopy. *Monthly Notices of the Royal Astronomical Society* 458 (3), 2657–2666.
- Benneke, B., Seager, S., 2012. Atmospheric Retrieval for Super-Earths: Uniquely Constraining the Atmospheric Composition With Transmission Spectroscopy. *The Astrophysical Journal* 753 (2), 100.  
 URL <http://arxiv.org/abs/1203.4018><http://dx.doi.org/10.1088/0004-637X/753/2/100>
- Berner, R. A., 2004. *The Phanerozoic Carbon Cycle: CO<sub>2</sub> and O<sub>2</sub>*. Oxford University Press, New York.
- Binney, J., Merrifield, M., 1998. *Galactic Astronomy*. Princeton University Press.
- Boschi, R., Lucarini, V., Pascale, S., Nov 2013. Bistability of the climate around the habitable zone: A thermodynamic investigation. *Icarus* 226 (2), 1724–1742.
- Boutle, I. A., Mayne, N. J., Drummond, B., Manners, J., Goyal, J., Hugo Lambert, F., Acreman, D. M., Earnshaw, P. D., may 2017. Exploring the climate of Proxima B with the Met Office Unified Model. *Astronomy & Astrophysics* 601 (2016), A120.  
 URL <http://arxiv.org/abs/1702.08463><http://dx.doi.org/10.1051/0004-6361/201630020><http://www.aanda.org/10.1051/0004-6361/201630020>
- Budyko, M. I., oct 1969. The effect of solar radiation variations on the climate of the Earth. *Tellus* 21 (5), 611–619.
- Charnay, B., Forget, F., Wordsworth, R., Leconte, J., Millour, E., Codron, F., Spiga, A., Sep 2013. Exploring the faint young Sun problem and the possible climates of the Archean Earth with a 3-D GCM. *Journal of Geophysical Research (Atmospheres)* 118 (18), 10,414–10,431.
- Checlair, J., Menou, K., Abbot, D. S., aug 2017. No Snowball on Habitable Tidally Locked Planets. *The Astrophysical Journal* 845 (2), 132.  
 URL <http://arxiv.org/abs/1705.08904><http://dx.doi.org/10.3847/1538-4357/aa80e1><http://stacks.iop.org/0004-637X/845/i=2/a=132?key=crossref.0179b453ba8de0d24a234f4256873009>

- Chemke, R., Kaspi, Y., 2017. Dynamics of Massive Atmospheres. *The Astrophysical Journal* 845 (1), 1.  
URL <http://dx.doi.org/10.3847/1538-4357/aa7742>
- Chemke, R., Kaspi, Y., Halevy, I., Nov 2016. The thermodynamic effect of atmospheric mass on early Earth's temperature. *Geophysical Research Letters* 43 (21), 11,414–11,422.
- Chen, H., Wolf, E. T., Kopparapu, R., Domagal-Goldman, S., Horton, D. E., nov 2018. Biosignature Anisotropy Modeled on Temperate Tidally Locked M-dwarf Planets. *The Astrophysical Journal* 868 (1), L6.  
URL <http://stacks.iop.org/2041-8205/868/i=1/a=L6?key=crossref.1bae0bdea0b2bbfa97039895721d00b8>
- Chen, H., Wolf, E. T., Zhan, Z., Horton, D. E., 2019. Habitability and Spectroscopic Observability of Warm M-dwarf Exoplanets Evaluated with a 3D Chemistry-Climate Model.  
URL <http://arxiv.org/abs/1907.10048>
- D'Errico, M., Faranda, D., Yiou, P., Nardini, C., Dec 2018. Detection and attribution of Southern European cold spells via a statistical Mechanics Approach. In: *AGU Fall Meeting Abstracts*. Vol. 2018. pp. GC21E–1138.
- Fraedrich, K., Jansen, H., Kirk, E., Luksch, U., Lunkeit, F., 2005. The Planet Simulator: Towards a user friendly model. *Meteorologische Zeitschrift* 14 (3), 299–304.
- Goldblatt, C., Claire, M. W., Lenton, T. M., Matthews, A. J., Watson, A. J., Zahnle, K. J., Dec 2009. Nitrogen-enhanced greenhouse warming on early Earth. *Nature Geoscience* 2 (12), 891–896.
- Gomez-Leal, I., Kaltenecker, L., Lucarini, V., Lunkeit, F., jan 2019. Climate Sensitivity to Carbon Dioxide and Moist Greenhouse threshold of Earth-like planets under an increasing solar forcing. *Icarus* 321, 608–618.  
URL <https://linkinghub.elsevier.com/retrieve/pii/S0019103517307820>  
<http://arxiv.org/abs/1901.02901>  
URL <http://dx.doi.org/10.3847/1538-4357/aaea5f>
- Haqq-Misra, J., Wolf, E. T., Joshi, M., Zhang, X., Kopparapu, R. K., jan 2018. Demarcating Circulation Regimes of Synchronously Rotating Terrestrial Planets within the Habitable Zone. *The Astrophysical Journal* 852 (2), 67.  
URL <http://arxiv.org/abs/1710.00435>  
<http://stacks.iop.org/0004-637X/852/i=2/a=67?key=crossref.31470b49165c69127c4c420f6aa490fe>
- Heng, K., Vogt, S. S., aug 2011. Gliese 581g as a scaled-up version of Earth: atmospheric circulation simulations. *Monthly Notices of the Royal Astronomical Society* 415 (3), 2145–2157.  
URL <https://academic.oup.com/mnras/article-lookup/doi/10.1111/j.1365-2966.2011.18853.x>
- Holden, P. B., Edwards, N. R., Fraedrich, K., Kirk, E., Lunkeit, F., Zhu, X., Sep 2016. PLASIM-GENIE v1.0: a new intermediate complexity AOGCM. *Geoscientific Model Development* 9, 3347–3361.
- Ingle, J. J., Crouch, S., 1 1988. Spectrochemical analysis.
- Johnson, B., Goldblatt, C., 2015. The nitrogen budget of Earth. *Earth-Science Reviews* 148, 150–173.
- Johnson, B., Goldblatt, C., sep 2017. A secular increase in continental crust nitrogen during the Precambrian. *Geochemical Perspectives Letters*, 24–28.  
URL <http://arxiv.org/abs/1709.02412>  
<http://dx.doi.org/10.7185/geochemlet.1731>  
<http://www.geochemicalperspectivesletters.org/article1731>
- Kaltenecker, L., Traub, W. A., Jucks, K. W., mar 2007. Spectral Evolution of an Earthlike Planet. *The Astrophysical Journal* 658 (1), 598–616.  
URL <https://doi.org/10.1086/122510>  
<http://stacks.iop.org/0004-637X/658/i=1/a=598>
- Koll, D. D. B., Cronin, T. W., 2019. Hot Hydrogen Climates near the inner edge of the Habitable Zone. *The Astrophysical Journal* 881 (2), 120.  
URL <http://arxiv.org/abs/1907.13169>
- Komacek, T. D., Abbot, D. S., feb 2019. The Atmospheric Circulation and Climate of Terrestrial Planets Orbiting Sun-like and M Dwarf Stars over a Broad Range of Planetary Parameters. *The Astrophysical Journal* 871 (2), 245.  
URL <http://arxiv.org/abs/1901.00567>  
<http://dx.doi.org/10.3847/1538-4357/aafb33>  
<http://stacks.iop.org/0004-637X/871/i=2/a=245?key=crossref.058e5787c42138cbe5ae3fc87aae806d>
- Kopparapu, R. K., Ramirez, R., Kasting, J. F., Eymet, V., Robinson, T. D., Mahadevan, S., Terrien, R. C., Domagal-Goldman, S., Meadows, V., Deshpande, R., 2013. Habitable Zones Around Main-Sequence Stars: New Estimates. *The Astrophysical Journal* 765 (2), 131.  
URL <http://stacks.iop.org/0004-637X/765/i=2/a=131?key=crossref.2f4b541791428841b8a64638c66c631c>
- Kopparapu, R. K., Ramirez, R. M., Schottelkotte, J., Kasting, J. F., Domagal-Goldman, S., Eymet, V., 2014. Habitable zones around main-sequence stars: Dependence on planetary mass. *Astrophysical Journal Letters* 787 (2), 1–14.
- Li, K.-F., Pahlevan, K., Kirschvink, J. L., Yung, Y. L., Jun 2009. Atmospheric pressure as a natural climate regulator for a terrestrial planet with a biosphere. *Proceedings of the National Academy of Science* 106 (24), 9576–9579.
- Manabe, S., Wetherald, R. T., 1975. The effects of doubling the CO<sub>2</sub> concentration on the climate of a general circulation model. *Journal of the Atmospheric Sciences* 32 (1), 3–15.  
URL [https://doi.org/10.1175/1520-0469\(1975\)032<0003:TEODTC>2.0.CO;2](https://doi.org/10.1175/1520-0469(1975)032<0003:TEODTC>2.0.CO;2)
- Menou, K., aug 2013. WATER-TRAPPED WORLDS. *The Astrophysical Journal* 774 (1), 51.  
URL <http://arxiv.org/abs/1304.6472>  
<http://dx.doi.org/10.1088/0004-637X/774/1/51>  
<http://stacks.iop.org/0004-637X/774/i=1/a=51?key=crossref.6afe4455e5ecb8ca63c9c618e09c6ec7>
- Nakajima, S., Hayashi, Y.-Y., Abe, Y., dec 1992. A Study on the Runaway Greenhouse Effect with a One-Dimensional Radiative Convective Equilibrium Model. *Journal of the Atmospheric Sciences* 49 (23), 2256–2266.  
URL [http://journals.ametsoc.org/doi/abs/10.1175/1520-0469\(1992\)049<2256:RAGHE>2.0.CO;2](http://journals.ametsoc.org/doi/abs/10.1175/1520-0469(1992)049<2256:RAGHE>2.0.CO;2)
- Nakayama, A., Kodama, T., Ikoma, M., Abe, Y., Jul 2019. Runaway climate cooling of ocean planets in the habitable zone: a consequence of seafloor weathering enhanced by melting of high-pressure ice. *arXiv e-prints*, arXiv:1907.00827.
- Nowajewski, P., Rojas, M., Rojo, P., Kimeswenger, S., May 2018. Atmospheric dynamics and habitability range in Earth-like aquaplanets obliquity simulations. *Icarus* 305, 84–90.
- Olson, S. L., Schwieterman, E. W., Reinhard, C. T., Lyons, T. W., mar 2018. Earth: Atmospheric Evolution of a Habitable Planet. In: *Handbook of*

- Exoplanets. Springer International Publishing, Cham, pp. 1–37.  
 URL [http://link.springer.com/10.1007/978-3-319-30648-3\(\\_ \)189-1](http://link.springer.com/10.1007/978-3-319-30648-3(_ )189-1)<http://arxiv.org/abs/1803.05967>[http://dx.doi.org/10.1007/978-3-319-30648-3\(\\_ \)189-1](http://dx.doi.org/10.1007/978-3-319-30648-3(_ )189-1)
- Oyama, V. I., Carle, G. C., Woeller, F., Pollack, J. B., Reynolds, R. T., Craig, R. A., 1980. Pioneer venus gas chromatography of the lower atmosphere of venus. *Journal of Geophysical Research: Space Physics* 85 (A13), 7891–7902.  
 URL <https://agupubs.onlinelibrary.wiley.com/doi/abs/10.1029/JA085iA13p07891>
- Paradise, A., Borth, H., Lunkeit, F., Kirk, E., Mar. 2019. alphaparrot/gplasmim: Radiative flexibility.  
 URL <https://doi.org/10.5281/zenodo.2602241>
- Paradise, A., Menou, K., 2017. GCM Simulations of Unstable Climates in the Habitable Zone. *The Astrophysical Journal* 848 (1), 33.  
 URL <http://dx.doi.org/10.3847/1538-4357/aa8blc>
- Pierrehumbert, R., 2005. Climate dynamics of a hard snowball earth. *Journal of Geophysical Research* 110 (D1), 1–22.
- Pierrehumbert, R., 2010. *Principles of Planetary Climate*. Cambridge University Press, New York.
- Pierrehumbert, R. T., Jan 2011. A Palette of Climates for Gliese 581g. *Astrophysical Journal Letters* 726 (1), L8.
- Ramirez, R., jul 2018. A More Comprehensive Habitable Zone for Finding Life on Other Planets. *Geosciences* 8 (8), 280.  
 URL <http://arxiv.org/abs/1807.09504><http://www.mdpi.com/2076-3263/8/8/280><http://www.mdpi.com/2076-3263/8/8/280>
- Ricchiazzi, P., Yang, S., Gautier, C., Sowle, D., oct 1998. SBDART: A Research and Teaching Software Tool for Plane-Parallel Radiative Transfer in the Earth's Atmosphere. *Bulletin of the American Meteorological Society* 79 (10), 2101–2114.  
 URL [http://journals.ametsoc.org/doi/abs/10.1175/1520-0477\(2018\)79%281998%29079%3C2101%3ASARATS%3E2.0.CO%3B2](http://journals.ametsoc.org/doi/abs/10.1175/1520-0477(2018)79%281998%29079%3C2101%3ASARATS%3E2.0.CO%3B2)
- Rybicki, G. B., Lightman, A. P., 2004. *Radiative Processes in Astrophysics*, 2nd Edition. Wiley-VCH, Weinheim.
- Sagan, C., Mullen, G., jul 1972. Earth and Mars: Evolution of Atmospheres and Surface Temperatures. *Science* 177 (4043), 52–56.  
 URL <https://science.sciencemag.org/content/177/4043/52><http://www.sciencemag.org/cgi/doi/10.1126/science.177.4043.52>
- Sasamori, T., Oct 1968. The Radiative Cooling Calculation for Application to General Circulation Experiments. *Journal of Applied Meteorology* 7 (5), 721–729.
- Sellers, W. D., 1969. A global climatic model based on the energy balance of the earth-atmosphere system. *Journal of Applied Meteorology* 8 (3), 392–400.  
 URL [https://doi.org/10.1175/1520-0450\(1969\)008<0392:AGCMBO>2.0.CO;2](https://doi.org/10.1175/1520-0450(1969)008<0392:AGCMBO>2.0.CO;2)
- Shields, A. L., Barnes, R., Agol, E., Charnay, B., Bitz, C., Meadows, V. S., jun 2016. The Effect of Orbital Configuration on the Possible Climates and Habitability of Kepler-62f. *Astrobiology* 16 (6), 443–464.  
 URL <http://arxiv.org/abs/1603.01272><http://dx.doi.org/10.1089/ast.2015.1353><http://online.liebertpub.com/doi/10.1089/ast.2015.1353>
- Snellen, I. A. G., de Kok, R., Birkby, J. L., Brandl, B., Brogi, M., Keller, C. U., Kenworthy, M., Schwarz, H., Stuik, R., 2015. Combining high-dispersion spectroscopy with high contrast imaging: Probing rocky planets around our nearest neighbors. *Astronomy & Astrophysics* 576 (3), A59.  
 URL <http://arxiv.org/abs/1503.01136><http://adsabs.harvard.edu/abs/2015A&A...576A..59S>
- Som, S. M., Buick, R., Hagadorn, J. W., Blake, T. S., Perreault, J. M., Harnmeijer, J. P., Catling, D. C., 2016. Earth's air pressure 2.7 billion years ago constrained to less than half of modern levels. *Nature Geoscience* 9 (6), 448–451.
- Strong, J., Plass, G. N., Nov. 1950. The Effect of Pressure Broadening of Spectral Lines on Atmospheric Temperature. *The Astrophysical Journal* 112, 365.
- Stüeken, E. E., Kipp, M. A., Koehler, M. C., Schwieterman, E. W., Johnson, B., Buick, R., 2016. Modeling pN<sub>2</sub> through Geological Time: Implications for Planetary Climates and Atmospheric Biosignatures. *Astrobiology* 16 (12), 33.  
 URL <http://arxiv.org/abs/1612.02865>
- Turbet, M., Leconte, J., Selsis, F., Bolmont, E., Forget, F., Ribas, I., Raymond, S. N., Anglada-Escudé, G., dec 2016. The habitability of Proxima Centauri b. *Astronomy & Astrophysics* 596, A112.  
 URL <http://arxiv.org/abs/1608.06919><http://www.aanda.org/10.1051/0004-6361/201629577>
- Valencia, D., Tan, V. Y. Y., Zajac, Z., Apr 2018. Habitability from Tidally Induced Tectonics. *The Astrophysical Journal* 857 (2), 106.
- Vladilo, G., Murante, G., Silva, L., Provenzale, A., Ferri, G., Ragazzini, G., feb 2013. The habitable zone of Earth-like planets with different levels of atmospheric pressure. *The Astrophysical Journal* 767 (1), 65.  
 URL <http://arxiv.org/abs/1302.4566><http://dx.doi.org/10.1088/0004-637X/767/1/65><http://stacks.iop.org/0004-637X/767/i=1/a=65?key=crossref.9d747f20949ec9f33cc162f00e5da089><http://arxiv.org/abs/1302.4566><http://dx.doi.org/10.1088/0004-637X/767/1/65>
- Walker, J., Hays, P., Kasting, J., 1981. A negative feedback mechanism for the long-term stabilization of earths surface temperature. *Journal of Geophysical Research* 86 (C10), 9776–9782.
- Way, M. J., Aleinov, I., Amundsen, D. S., Chandler, M. A., Clune, T. L., Genio, A. D. D., Fujii, Y., Kelley, M., Kiang, N. Y., Sohl, L., Tsigaridis, K., jul 2017. Resolving Orbital and Climate Keys of Earth and Extraterrestrial Environments with Dynamics (ROCKE-3D) 1.0: A General Circulation Model for Simulating the Climates of Rocky Planets. *The Astrophysical Journal Supplement Series* 231 (1), 12.  
 URL <http://stacks.iop.org/0067-0049/231/i=1/a=12?key=crossref.2440b27e9f0a7debc0b27c7bc18e2247>
- Wilcox, L. J., Hoskins, B. J., Shine, K. P., 2012. A global blended tropopause based on era data. part i: Climatology. *Quarterly Journal of the Royal Meteorological Society* 138 (664), 561–575.  
 URL <https://rmets.onlinelibrary.wiley.com/doi/abs/10.1002/qj.951>
- Williams, D. M., Kasting, J. F., sep 1997. Habitable Planets with High Obliquities. *Icarus* 129 (1), 254–267.  
 URL <http://www.sciencedirect.com/science/article/pii/S0019103597957596><https://linkinghub.elsevier.com/retrieve/pii/S0019103597957596>

- Wolf, E., Toon, O., 2014. Controls on the Archean climate system investigated with a global climate model. *Astrobiology* 14 (3), 241–253, PMID: 24621308.  
URL <https://doi.org/10.1089/ast.2013.1112>
- Wolf, E. T., apr 2017. Assessing the Habitability of the TRAPPIST-1 System Using a 3D Climate Model. *The Astrophysical Journal* 839 (1), L1.  
URL <http://arxiv.org/abs/1703.05815><http://dx.doi.org/10.3847/2041-8213/aa693a><http://stacks.iop.org/2041-8205/839/i=1/a=L1?key=crossref.1f8babc828488896844eaa0df54a6712>
- Wordsworth, R., aug 2016. Atmospheric nitrogen evolution on Earth and Venus. *Earth and Planetary Science Letters* 447, 103–111.  
URL <https://linkinghub.elsevier.com/retrieve/pii/S0012821X16301583>
- Wordsworth, R., Pierrehumbert, R., 2014. Abiotic oxygen-dominated atmospheres on terrestrial habitable zone planets. *Astrophysical Journal Letters* 785 (2), 2–5.
- Yang, J., Cowan, N. B., Abbot, D. S., 2013. Stabilizing Cloud Feedback Dramatically Expands the Habitable Zone of Tidally Locked Planets. *The Astrophysical Journal* 771 (2), L45.  
URL <http://stacks.iop.org/2041-8205/771/i=2/a=L45?key=crossref.dad84a2284f357b75182157e7808b044>
- Yang, J., Liu, Y., Hu, Y., Abbot, D. S., 2014. Water trapping on tidally locked terrestrial planets requires special conditions. *Astrophysical Journal Letters* 796 (2), 2–7.
- Zahnle, K., Buick, R., may 2016. Ancient air caught by shooting stars. *Nature* 533 (7602), 184–186.  
URL <http://www.nature.com/articles/533184a>